Journal of Zhejiang University-SCIENCE A (Applied Physics & Engineering)
ISSN 1673-565X (Print); ISSN 1862-1775 (Online)
www.jzus.zju.edu.cn; link.springer.com
E-mail: jzus_a@zju.edu.cn

Wave filtering and firing modes in a light-sensitive neural circuit*

Xiu-fang ZHANG[1], Jun MA[†‡1,2]

[1]*Department of Physics, Lanzhou University of Technology, Lanzhou 730050, China*

[2]*School of Science, Chongqing University of Posts and Telecommunications, Chongqing 430065, China*

[†]E-mail: hyperchaos@163.com

Received July 13, 2021; Revision accepted Aug. 5, 2021; Crosschecked Sept. 4, 2021

Abstract: Inspired by the photoelectric effect, a phototube is incorporated into a simple neural circuit, and then the output voltage and dynamics become sensitive to external illumination within a specific frequency band. The firing modes are also dependent on the amplitude and frequency band in the illumination. In this paper, the signal outputs from a chaotic circuit are used as external optical signals, which are filtered and encoded by a phototube. Then, the functional neural circuit is excited to present a variety of firing modes and patterns. An exponential function of the filtering wave is proposed to discover the biophysical mechanism for frequency selection in the retina as most of wave bands of the external illumination are absorbed in the cathode material of the phototube while a specific band is effective in inducing a photocurrent for stimulating the visual neurons. Based on our light-sensitive neural circuit and model, external illumination is filtered and firing modes in the neuron are reproduced; furthermore, the mode transition induced by parameter shift is also investigated in detail. This result discovers the signal processing mechanism in the visual neurons and provides helpful guidance for designing artificial sensors for encoding optical signals and for repairing abnormalities in the retina of the visual system.

Key words: Light-sensitive neuron; Neural circuit; Phototube; Bifurcation; Information encoding
https://doi.org/10.1631/jzus.A2100323 **CLC number:** O59; TN710

1 Introduction

Neurons from different functional regions in the brain can perceive and encode a variety of external stimuli and the nervous system is then excited to guide the most suitable gaits in the body. The auditory neurons (Machens et al., 2003; Heil, 2004; Koundakjian et al., 2007; Richter et al., 2008; Zhou et al., 2021a) can detect acoustic waves; the thermosensitive neurons (Nakayama, 1985; Zhang et al., 2004; Lee and Kenyon, 2009; Ruchty et al., 2010; Xu et al., 2020a) can discern changes of temperature; the visual neurons (Gabbiani et al., 2002; Peron and Gabbiani, 2009; Furtak et al., 2012; Wiederman and O'Carroll, 2013; Dipoppa et al., 2018) can perceive optical signals and light. Indeed, the activation and release of biophysical functions in nervous systems are associated with the neural activities of neurons and astrocytes (Li et al., 2016; Tang et al., 2017; Brazhe et al., 2018; Erkan et al., 2019; Du et al., 2020), while the collective behaviors and firing modes in neural networks are controlled by local kinetics and the links of nodes as well (Lv et al., 2019; Duan et al., 2020; Jiao et al., 2020; Yao, 2020; Zandi-Mehran et al., 2020). From a dynamical viewpoint, the local kinetics of the network can be described by many generic neurons, and even mathematical neurons. As a result, the coupling channels and external stimuli can be adjusted to trigger regular spatial patterns and ordered waves, and synchronization stability can also be controlled completely. In fact, neurons from different regions of the brain can develop specific functions and become sensitive to

‡ Corresponding author
* Project supported by the National Natural Science Foundation of China (No. 12072139)
ORCID: Jun MA, https://orcid.org/0000-0002-6127-000X

specific stimuli for generating appropriate firing modes even in the presence of noise. Some interneurons develop autapse connections (Seung et al., 2000; Song et al., 2019; Zhao et al., 2020; Li et al., 2021) and this self-adaption is enhanced by bridging an auxiliary loop when neurons are injured along the axon (Wang et al., 2017). When autapse connection is activated in a local area of the network, the switch between excitatory and inhibitory autapse will induce pacing stimulus and defects blocking in the wave propagation (Qin et al., 2014; Ma et al., 2015; Ge et al., 2019; Yao et al., 2019; Baysal et al., 2021), and so the collective behaviors of neural networks are regulated completely. On the other hand, the involvement of astrocytes (Achour and Pascual, 2012; MacVicar and Newman, 2015; Guo et al., 2017) connecting to neurons or the neural network will change the firing patterns in neural activities because calcium flow is changed to regulate the channel current and membrane potentials. Thus, the estimation and regulation of biological neurons and the neural network become a challenge when the biophysical effect and anatomic structure are considered (Ma et al., 2019).

The functional biophysical neuron (Wu et al., 2020) can be sensitive to specific stimuli, and similar dynamical properties can be reproduced in a large number of neural circuits by incorporating specific electric components into them. For the human auditory system, sound voice with the frequencies of 20 to 20 000 Hz can be heard effectively while bats are more sensitive in the ultrasonic. For the human visual system, light and illumination within the frequency band from 380 to 750 THz can be detected and, in particular, human eyes are most sensitive to green light with a wavelength of 500 to 560 nm. Therefore, specific electric components can be designed to enable the release and conversion of energy from external stimuli. For example, a memristor can be connected to a nonlinear circuit (Fitch et al., 2012; Vourkas and Sirakoulis, 2016; Babacan et al., 2017; Bao H et al., 2020; Bao BC et al., 2021), and then memristive synapse (Juzekaeva et al., 2019; Wu et al., 2019; Chen et al., 2020) is obtained and its dynamics relies on the initial value for the memory variable (magnetic flux). Connection of a thermistor to the nonlinear circuit (Lukić and Denić, 2015; Ibrahim et al., 2019; Xu et al., 2020b) makes its dynamics become sensitive to the temperature because its channel current is adjusted by the external temperature. The channel current across the Josephson junction (Saira et al., 2016; Pountougnigni et al., 2019; Koudafokê et al., 2021) can be regulated by an external magnetic field, and its involvement (Zhang et al., 2020, 2021) in the nonlinear circuit can enhance its ability to detect slight changes in the magnetic field. The coupling channel can also be controlled by an external field when a Josephson junction is used to connect neural circuits. A phototube can realize effective conversion from optical signals to electric signals, so the nonlinear circuit excited by a photocurrent (Liu et al., 2020a, 2020b) can be used to reproduce similar behaviors in eyes and visual system.

In this paper, a feasible light-sensitive neural circuit is proposed to discern how the external electromagnetic wave is filtered in the suggested frequency band for generating an effective photocurrent along the branch circuit. External illumination can be converted into an equivalent electric stimulus via the retina and then the visual neurons are excited for further information processing in the nervous system. Thus, the retina can be considered as an effective photoelectric converter and a phototube can be used to reproduce a similar biophysical function in light-sensitive neural circuits. The simple neural circuit is composed of a capacitor, an induction coil, a nonlinear resistor, and two linear resistors, and then a phototube is connected to enhance its dynamic dependence on external illumination. The phototube has two functional roles, wave filtering and photoelectric conversion, and then the equivalent neural circuit can be used to model the biophysical function and processing signal in visual neurons. The criterion for frequency selection in the electric component for wave filtering is suggested, and the filtered illumination can induce continuous electric stimulus in the neural circuit. The voltage outputs from a chaotic circuit are used as a realistic optical signal for activating the phototube; the photocurrent across the phototube is controlled under the suggested criterion for wave filtering. Furthermore, the functional neural circuit is excited to reproduce similar firing modes from biological visual neurons and the Hamilton

energy is estimated when the firing modes are changed.

2 Model and scheme

As mentioned above, the eyes and visual neuron can perceive external illumination, and electromagnetic waves within specific frequency bands can be captured and converted to electric stimuli via the retina. The photoelectric conversion is realized via the phototube when external illumination is applied with high frequency beyond the threshold decided by the cathode material; the functional neural circuit coupled by a phototube is shown in Fig. 1.

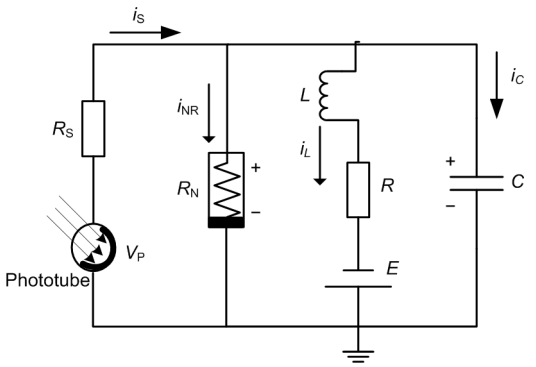

Fig. 1 Schematic diagram for a light-sensitive neural circuit controlled by the photocurrent across the phototube
V_P, C, L, R, R_S, R_N, and E represent the output voltage across the phototube, capacitor, inductor, linear resistors, nonlinear resistor, and constant voltage source, respectively. i_S, i_{NR}, i_L, and i_C represent the channel currents along the linear resistors, nonlinear resistor, induction coil L, and capacitor C, respectively

Guided by Kirchhoff's law, the circuit equations for Fig. 1 are obtained by

$$\begin{cases} C\dfrac{\mathrm{d}V}{\mathrm{d}t} = i_S - i_L - i_{NR}, \\ L\dfrac{\mathrm{d}i_L}{\mathrm{d}t} = V - Ri_L + E, \end{cases} \tag{1}$$

where the photocurrent across the phototube is described by $i_S=(V_P-V)/R_S$. V defines the voltage for the capacitor C. The channel current (Kyprianidis et al., 2012) across the nonlinear resistor R_N is estimated by

$$i_{NR} = -\frac{1}{\rho}\left(V - \frac{V^3}{3V_0^2}\right), \tag{2}$$

where the parameters ρ and V_0 represent the resistance in the linear region and the cut-off voltage for the nonlinear resistor, respectively. The phototube is used as a voltage source V_P when a large resistance is applied in the resistor R_S. In addition, the phototube can also be considered as a current source i_S when the linear resistor R_S is selected within a finite resistance, and then the photocurrent (Liu et al., 2020a) can be approached by

$$i_S = \frac{2I_H}{\pi}\arctan(V_P - V_a), \tag{3}$$

where I_H and V_a denote the saturation current (maximal current value) and the reverse cut-off voltage, which can block the photocurrent across the phototube, respectively.

Firstly, we consider the case that the phototube is activated as the voltage source and a standard scale transformation (Wang et al., 2019) is applied for the physical variables and parameters in Eqs. (1)–(3) as follows:

$$\begin{aligned} &x = \frac{V}{V_0}, \quad y = \frac{\rho i_L}{V_0}, \quad u_s = \frac{\rho V_P}{R_S V_0}, \quad \tau = \frac{t}{\rho C}, \\ &a = \frac{E}{V_0}, \quad b = \frac{R}{\rho}, \quad c = \frac{\rho^2 C}{L}, \quad \xi = \frac{\rho}{R_S}. \end{aligned} \tag{4}$$

Thus, the dimensionless light-sensitive neuron can be described by

$$\begin{cases} \dfrac{\mathrm{d}x}{\mathrm{d}\tau} = x(1-\xi) - \dfrac{1}{3}x^3 - y + u_s, \\ \dfrac{\mathrm{d}y}{\mathrm{d}\tau} = c(x + a - by), \end{cases} \tag{5}$$

where the variables x, y, and u_s represent the membrane potential, recovery variable for slow current, and external stimulus from the phototube, respectively. Indeed, the phototube is sensitive to specific bands of external illumination and electromagnetic waves, and its amplitude is related to the frequency as follows:

$$u_s = A(\omega)\cos(2\pi\omega\tau), \tag{6a}$$

$$A(\omega) = \begin{cases} A_0 \exp(-\tau/\lambda), & \omega \geq \omega_{\max}, \\ A_0, & \omega_{\min} < \omega < \omega_{\max}, \\ A_0 \exp(-\tau/\lambda), & \omega \leq \omega_{\min}, \end{cases} \tag{6b}$$

where the normalized parameter λ is considered as a decay factor, and is related to the properties of the cathode material of the phototube. The parameter λ can be controlled by using different coating materials while the parameters ω and A_0 control the main frequency and amplitude in the filtered wave and voltage source, respectively. Some optical signals within specific bands of frequency will be absorbed and decayed via the phototube, and a lower value for the decay factor λ means that the external illumination can be suppressed quickly. In addition, $\omega_{\min}$ and $\omega_{\max}$ define respectively the upper and lower limit thresholds for the frequency. As a result, the electromagnetic wave is filtered and its frequency remains active in the region [$\omega_{\min}$, $\omega_{\max}$], and the phototube is then activated effectively. In the experimental way, the equivalent voltage source u_s across the phototube can be approached by using the Heaviside function $H(\cdot)$ as follows:

$$\begin{aligned} u_s &= A(\omega)\cos(2\pi\omega\tau) \\ &= [H(\omega-\omega_{\max}) + H(\omega_{\min}-\omega)]A_0 \exp\left(-\frac{\tau}{\lambda}\right) \\ &\quad \times \cos(2\pi\omega\tau) + [H(\omega_{\max}-\omega)H(\omega-\omega_{\min})] \\ &\quad \times A_0 \cos(2\pi\omega\tau). \end{aligned} \tag{7}$$

Indeed, the phototube can also be activated as a current source, and the photocurrent defined in Eq. (3) can be approached by using a simple dimensionless form as follows:

$$i_S = I_0 \arctan(x - u_a), \tag{8}$$

where I_0 is the maximum value of the dimensionless photocurrent, and the normalized parameter u_a is related to the material property of the phototube. In this way, the functional neuron driven by the photocurrent can be obtained by

$$\frac{\mathrm{d}x}{\mathrm{d}\tau} = x - \frac{1}{3}x^3 - y + i_S, \tag{9a}$$

$$\frac{\mathrm{d}y}{\mathrm{d}\tau} = c(x + a - by). \tag{9b}$$

As is well known, the induction coil and capacitor of the neural circuit can pump and release field energy (Zhou et al., 2021b). The inner energy in the neural circuit is propagated and exchanged between electric components (capacitor and induction coil) when the output voltage is changed with the change of channel current across the induction coil as follows:

$$\begin{aligned} W &= \frac{1}{2}CV^2 + \frac{1}{2}Li_L^2 \\ &= CV_0^2\left(\frac{1}{2}x^2 + \frac{1}{2c}y^2\right) = CV_0^2 H. \end{aligned} \tag{10}$$

By applying similar scale transformation for the variables and parameters in the field energy shown in Eq. (10), the dimensionless Hamilton energy H for the functional neuron is updated as follows:

$$H = \frac{1}{2}x^2 + \frac{1}{2c}y^2. \tag{11}$$

The realistic optical signal and electromagnetic wave show a wide band in frequency, and the output voltages from chaotic circuits meet this requirement. For simplicity but without losing generality, the output voltages from Pikovskii-Rabinovich (PR) (Pikovskii and Rabinovich, 1978) are used as a light signal, and their dynamics are described by

$$\begin{cases} \dfrac{\mathrm{d}x'}{\mathrm{d}\tau} = y' - \delta z', \\ \dfrac{\mathrm{d}y'}{\mathrm{d}\tau} = -x' + 2\gamma y' + \alpha z' + \beta, \\ \dfrac{\mathrm{d}z'}{\mathrm{d}\tau} = \mu(x' + z' - z'^3), \end{cases} \tag{12}$$

where the variables x', y', and z' can be mapped from the channel currents across the induction coil and the voltages across the capacitors in the chaotic circuit; the normalized parameters are selected as α=0.165, β=0, γ=0.201, δ=0.66, and μ=1/0.047. In the next section, initial values are fixed at (0.1, 0.1, 0.1), and a chaotic series for variable x' is used as an external

signal source which will be filtered and encoded by the phototube and an effective photocurrent is triggered to regulate the firing modes and patterns from the light-sensitive neuron.

3 Numerical results and discussion

The fourth-order Runge-Kutta algorithm is applied to find numerical solutions for the neuron model with time step h=0.01, the initial value for the neuron model is selected as (0.2, 0.1), and the transient period is about 1000 time units. The chaotic series from the chaotic PR system are used as an unfiltered signal (electromagnetic wave) or a realistic illumination signal. In Fig. 2, chaotic series x' are presented and filtered.

From Fig. 2, the criterion for wave filtering plays an important role in frequency selection. As a result, the filtered wave shows a distinct difference in profile from the original signal source and the frequency band is kept in the region [$\omega_{\min}$, $\omega_{\max}$]; further decrease of the decay factor λ can enhance the effect of wave filtering. Furthermore, the filtered wave is used to activate the functional neuron and the dynamics' dependence on the main frequency ω in the voltage source across the phototube. The results are plotted in Fig. 3.

The isolated neuron can present periodic firing at ω<0.14, and chaotic firing patterns are induced at 0.14<ω<0.17. When the wave filtering and frequency selection are switched on, the signal series with low frequency and high frequency are filtered from the chaotic signal source. The cone cells are of three

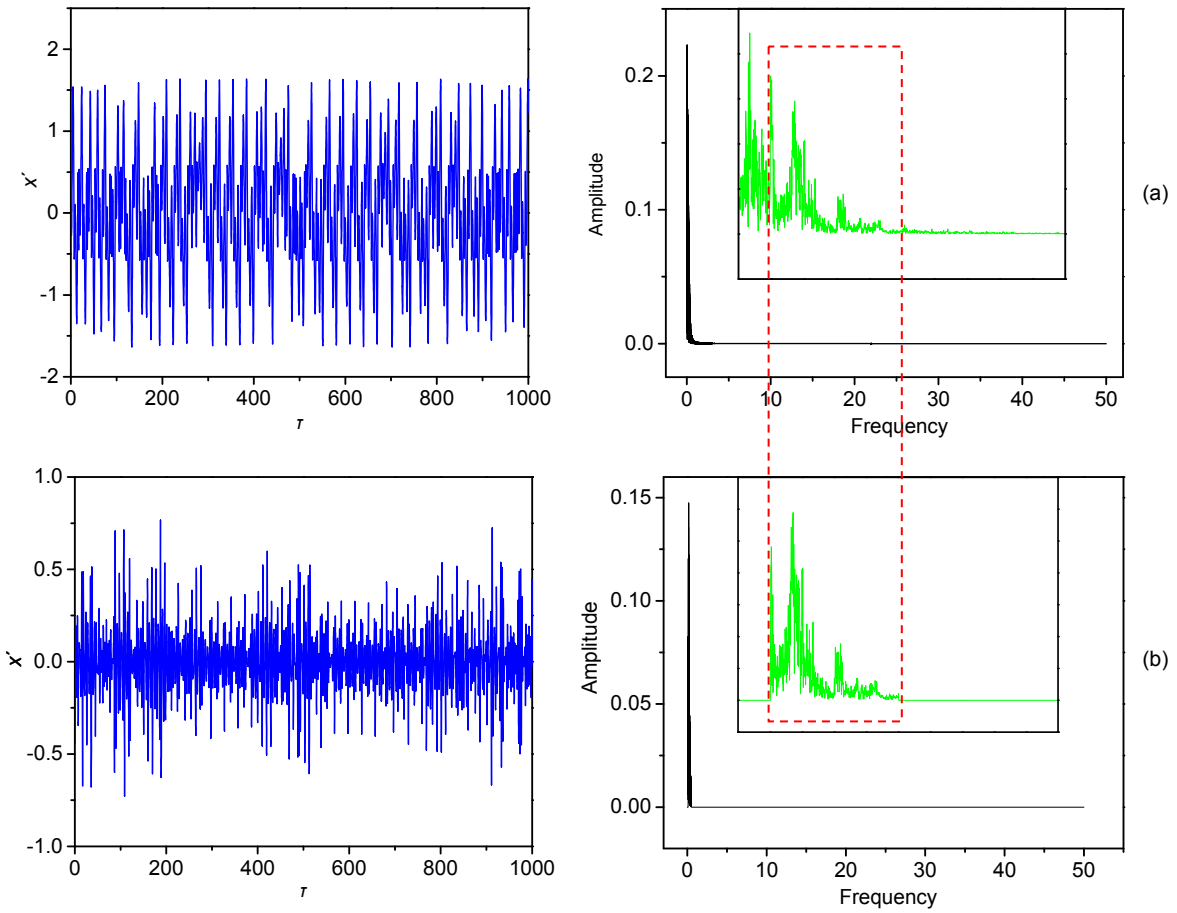

Fig. 2 Wave filtering and the power spectrum for the chaotic signals and filtered signals: (a) original chaotic series and power spectrum via fast Fourier transform (FFT); (b) filtered signal source and power spectrum. The thresholds for frequency selection and parameters are fixed at $\omega_{\min}$=0.1, $\omega_{\max}$=0.5, a=0.7, b=0.8, c=0.1, ξ=0.175, and λ=5. The inserted subfigure is an enlarged version and the frequency region is within [0.0, 1.0]

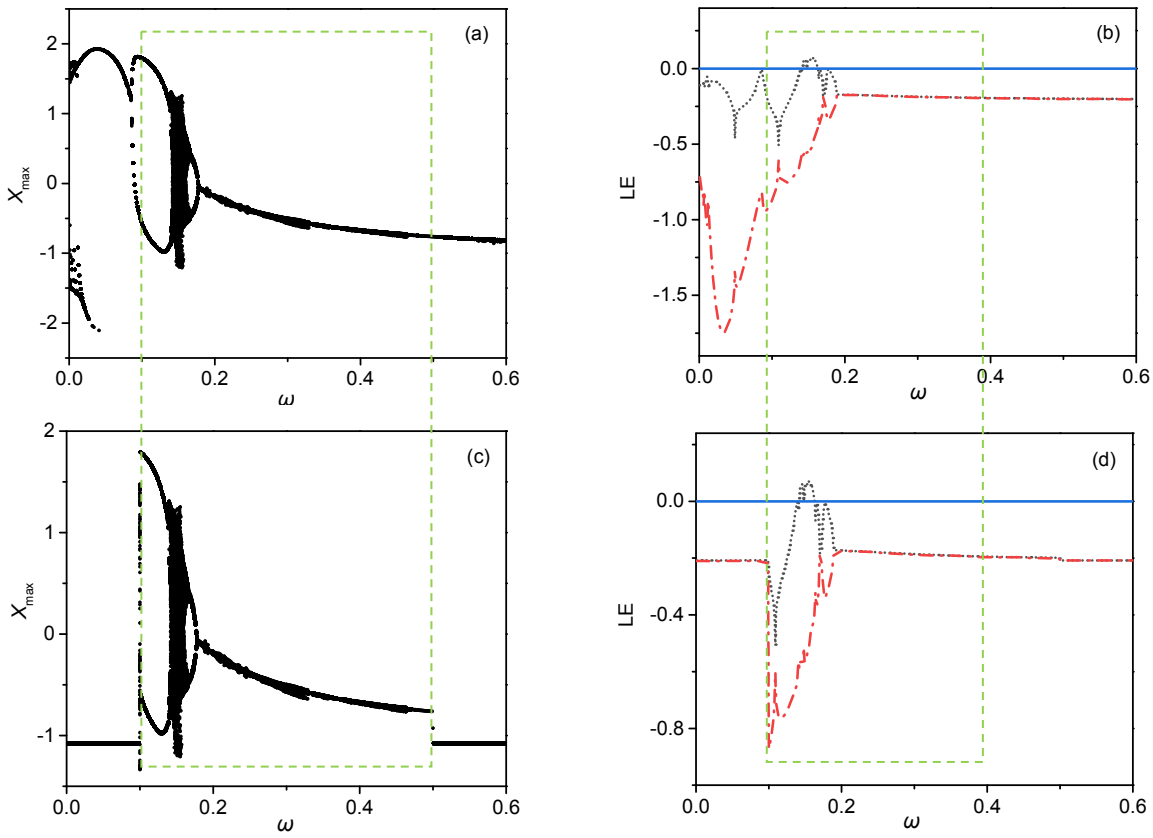

Fig. 3 Dependence of firing mode and Lyapunov exponent (LE) spectrum on the frequency in the voltage source u_s: bifurcation analysis for membrane potential (a) and LE spectra (b) for an isolated neuron driven by voltage source u_s=Acos(2π$\omega\tau$) without wave filtering; bifurcation analysis for membrane potential (c) and LE spectra (d) for an isolated neuron driven by u_s=$A(\omega)$cos(2π$\omega\tau$) under wave filtering. The thresholds for frequency selection and parameters are fixed at ω_{min}=0.1, ω_{max}=0.5, a=0.7, b=0.8, c=0.1, ξ=0.175, λ=5, and A=0.9

kinds and they can perceive the electromagnetic waves as long wavelength, moderate wavelength, and short wavelength. For biological neurons, the excitability can be controlled by external stimuli and then appropriate firing modes are stabilized in the neural activities. Therefore, we will discuss three cases in which the optical signal and illumination are presented with low frequency, moderate frequency, and high frequency, respectively. First, we discuss the case for low frequency and the thresholds are selected as ω_{min}=0.005, ω_{max}=0.16. In Fig. 4, the spectra for the signal source before and after wave filtering, and the phase portraits are plotted.

When the voltage source after wave filtering is kept in the low frequency band, the combined electric stimuli can induce firing patterns within multiple modes. That is different from the case where the neuron is excited by a sole periodic forcing current with low frequency. Thus, the filter wave criterion and mechanism make the functional neuron present rich firing modes and patterns under excitation from the filtered wave with combined signals.

In the case of moderate frequency, the thresholds for frequency selection are fixed at ω_{min}=0.16, ω_{max}=0.3, and the results are presented in Fig. 5.

With moderate frequency in the source signal across the phototube, the photocurrent can enhance chaotic firing patterns effectively, and chaotic attractors are formed in the phase space.

The case of high frequency, with the threshold ω_{min}=0.3, ω_{max}=0.5, is calculated in Fig. 6.

Similar to the results in Fig. 5, the firing patterns in the electric activities show a chaotic series, and attractors are formed completely when a filtered wave with high frequency is used to activate a similar voltage source across the phototube with high frequency. As mentioned above, the Hamilton energy is dependent on the membrane potential and channel

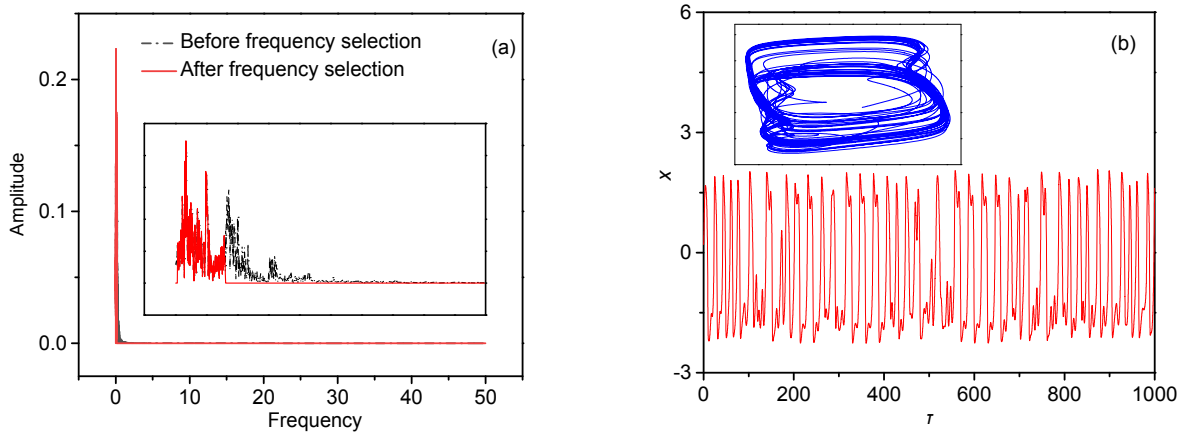

Fig. 4 Frequency domain for exciting signals and phase portraits for the neuron: (a) frequency domain for voltage source with and without wave filtering; (b) phase portraits and firing patterns with wave filtering at ω_{min}=0.005, ω_{max}=0.16. The parameters are fixed at a=0.7, b=0.8, c=0.1, ξ=0.175, and λ=5

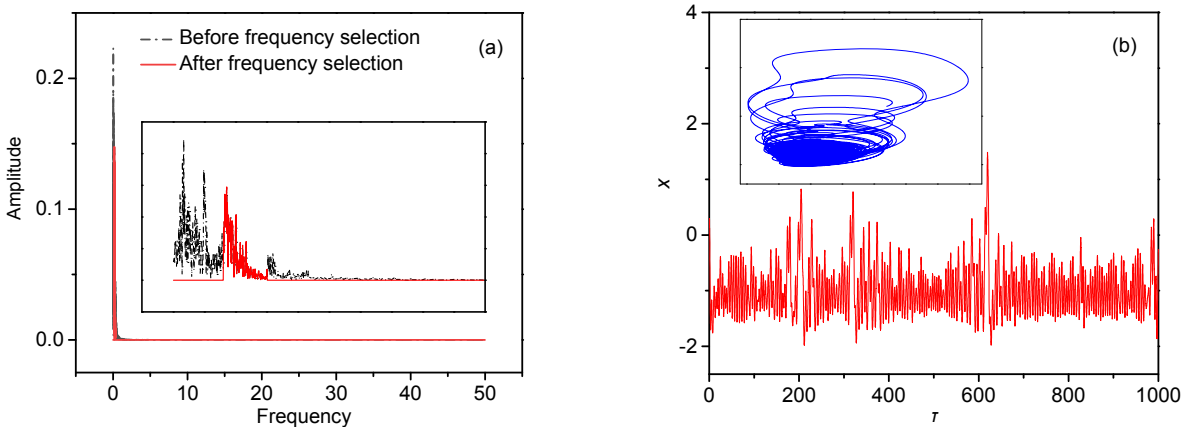

Fig. 5 Frequency domain for exciting signals and phase portraits for the neuron: (a) frequency domain for voltage source with and without wave filtering; (b) phase portraits and firing patterns with wave filtering at ω_{min}=0.16, ω_{max}=0.3. The parameters are fixed at a=0.7, b=0.8, c=0.1, ξ=0.175, and λ=5

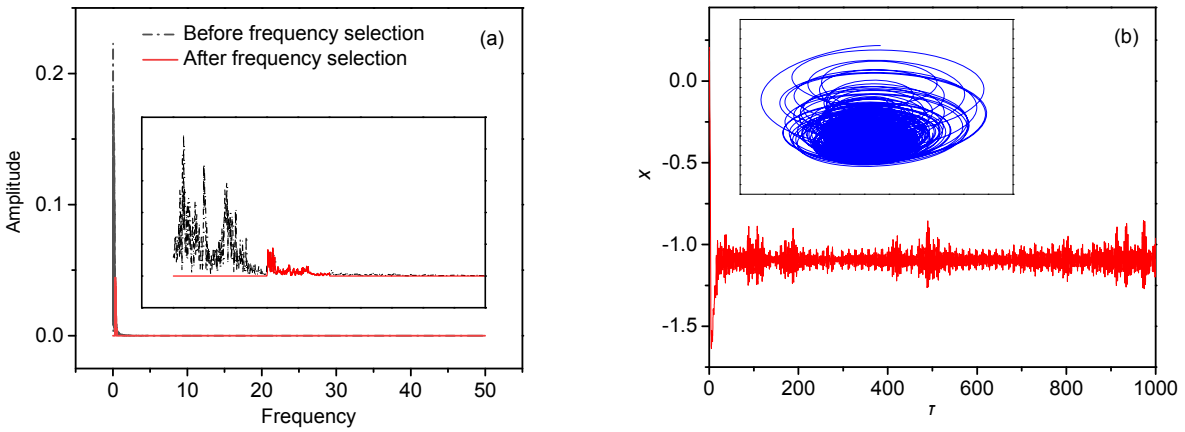

Fig. 6 Frequency domain for exciting signals and phase portraits for the neuron: (a) frequency domain for voltage source with and without wave filtering; (b) phase portraits and firing patterns with wave filtering at ω_{min}=0.3, ω_{max}=0.5. The parameters are fixed at a=0.7, b=0.8, c=0.1, ξ=0.175, and λ=5. The inserted subfigure in Fig. 6a is an enlarged one in the region of frequency [0.0, 1.0]

current, and any changes in the firing modes will change the Hamilton energy. In Fig. 7, the evolution of Hamilton energy is calculated to discern the effect of wave filtering in the electromagnetic wave imposed on the phototube.

As shown by the dashed line in Fig. 7a, the neural circuit is excited by a chaotic series as $u_s=x'(\tau)$, and the neuron energy shows multiple modes and its evolution is changed greatly when wave filtering is switched on. In addition, the fluctuation range of Hamilton energy is decreased when the voltage source with moderate or high frequency is applied to trigger chaotic firing patterns in the electric activities. That is, chaotic firing modes make neurons show lower Hamilton energy. On the other hand, as shown in Eq. (11), any changes in the intrinsic parameter c will change the energy directly, and any changes in the intrinsic parameters (a, b, c, ξ) will change the firing mode, and the energy in the neural circuit is regulated subsequently. In Fig. 8, the sole periodic electric stimulus from the phototube as $u_s=A\cos(\omega\tau)$

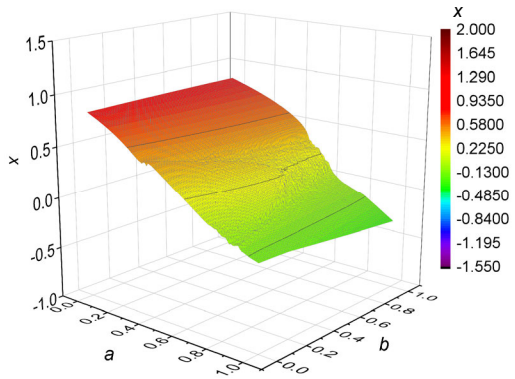

Fig. 8 Evolution of membrane potentials in the two-parameter space (membrane potentials for variable x in the neuron driven by periodic stimulus $u_s=A\cos(\omega\tau)$, with the parameters fixed at A=0.9, ω=0.16, c=0.1, and ξ=0.175)

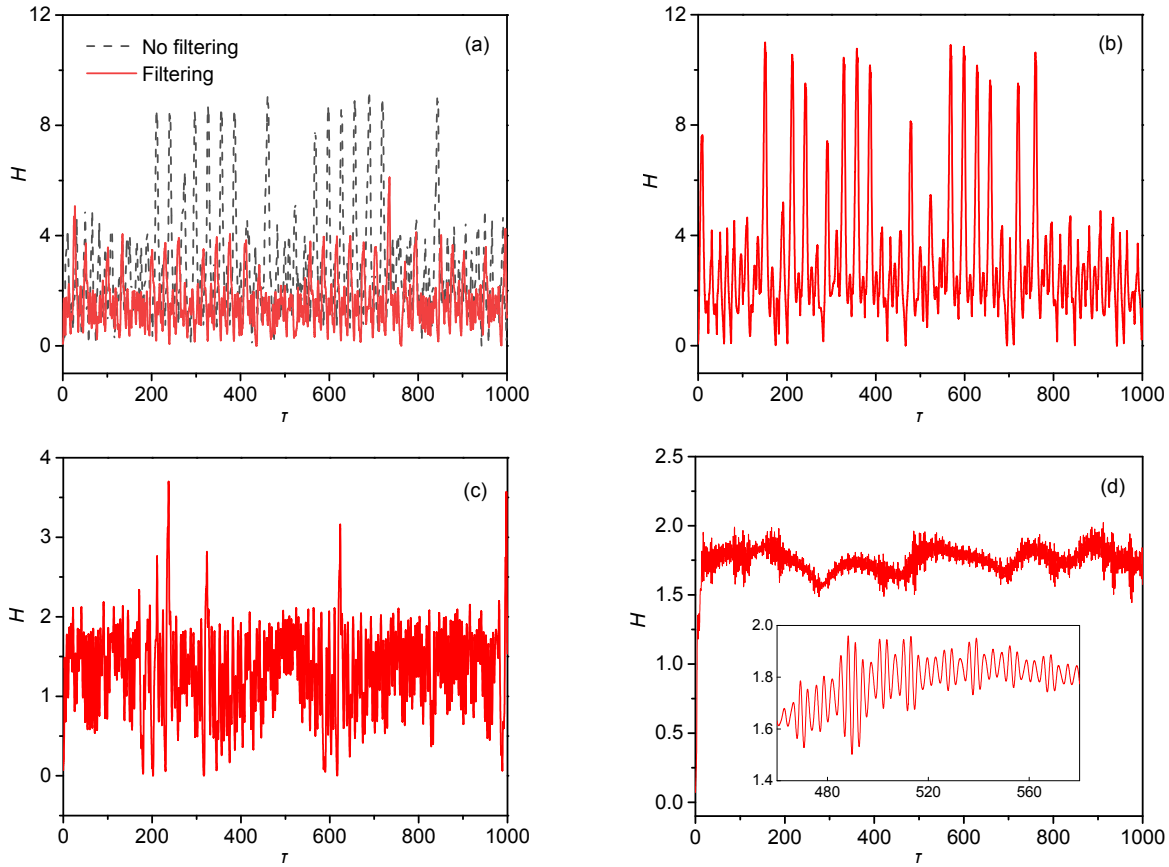

Fig. 7 Energy pumping and release in the functional neuron with and without wave filtering under different thresholds in frequency: (a) ω_{min}=0.1, ω_{max}=0.5; (b) ω_{min}=0.005, ω_{max}=0.16; (c) ω_{min}=0.16, ω_{max}=0.3; (d) ω_{min}=0.3, ω_{max}=0.5. The parameters are fixed at a=0.7, b=0.8, c=0.1, ξ=0.175, and λ=5. The dashed line describes the evolution of Hamilton energy in the neuron driven by chaotic signals without wave filtering, and the solid lines represent the energy series under wave filtering with different thresholds

is applied to detect the mode dependence of membrane potential x on the intrinsic parameters (a, b).

For greater clarity, the bifurcation analysis is calculated in Fig. 9 by changing one of the intrinsic parameters in the neural circuit driven by periodic stimulus. When the parameter b is fixed, in case of a periodic stimulus, the neuron shows a distinct transition from periodic firing to chaotic firing at a=0.46 and then the chaos is suppressed at a=0.8 for retrieving periodic firing modes. When the parameter a is fixed, the neuron driven by periodic forcing goes through periodic firing to chaotic firing modes from b=0.54, and further increase of the parameter b will wake periodic firing completely. In Fig. 10,

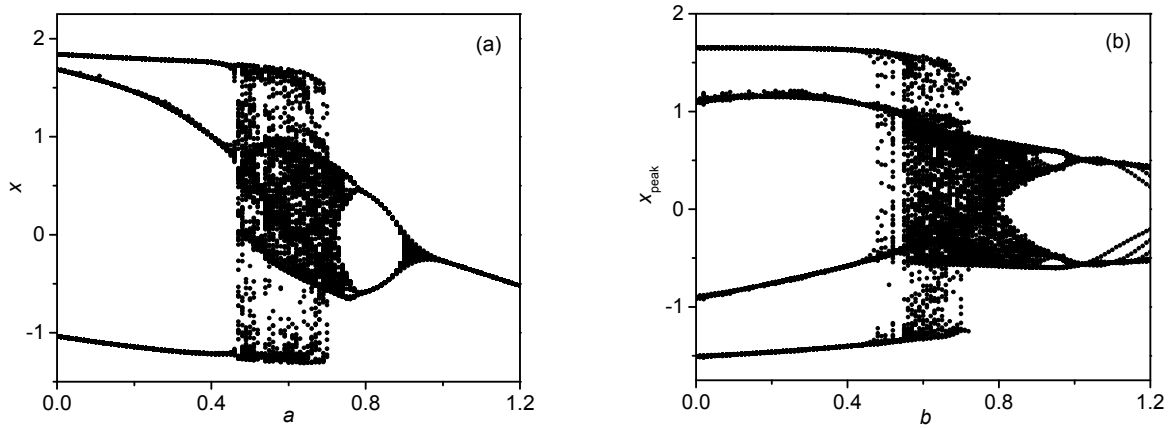

Fig. 9 Bifurcation diagrams for membrane potential x by changing one intrinsic parameter: (a) b=0.7; (b) a=0.7. The parameters are fixed at A=0.9, ω=0.16, c=0.1, and ξ=0.175

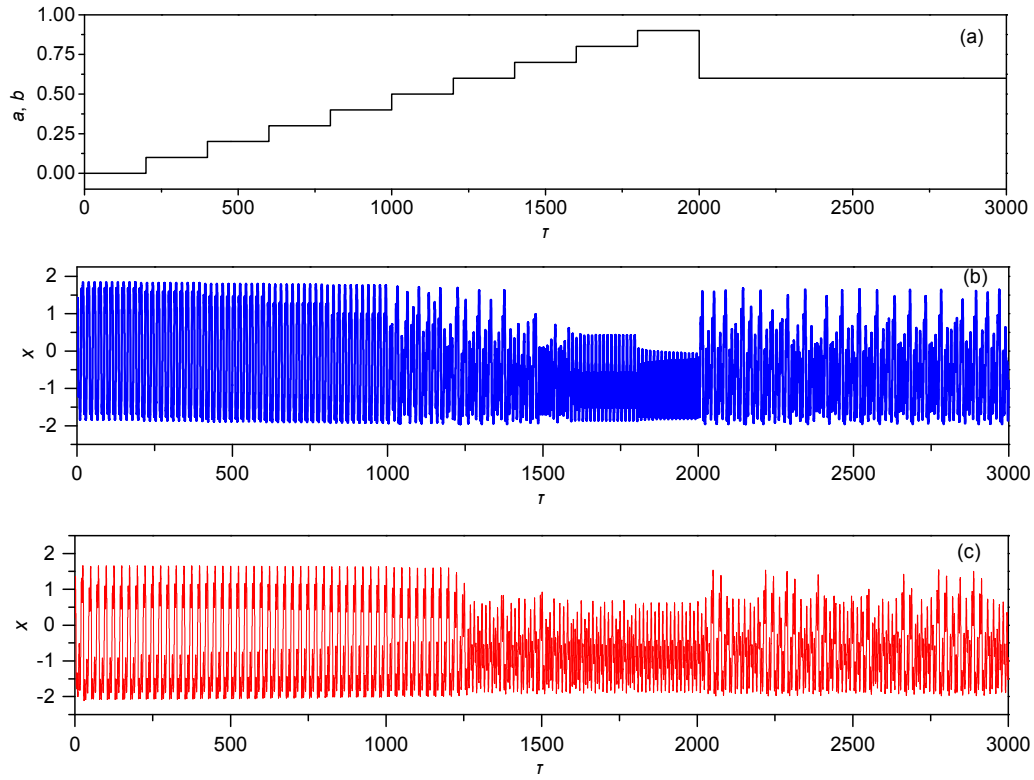

Fig. 10 Firing patterns in electric activities when two intrinsic parameters are jumped: (a) parameters jumping in constant steps with time; (b) jumped parameter a with fixed b=0.7; (c) jumped parameter b with fixed a=0.7. The other parameters are fixed at A=0.9, ω=0.16, c=0.1, and ξ=0.175

the evolution of membrane potential is plotted when one intrinsic parameter is jumped with a constant step.

Indeed, any changes in one of the intrinsic parameters will induce distinct mode transition in the neural activities when periodic stimulus from the phototube is applied. Furthermore, we consider the case when the phototube is activated and it is used as current source; the firing mode's dependence on intrinsic parameters is plotted in Fig. 11.

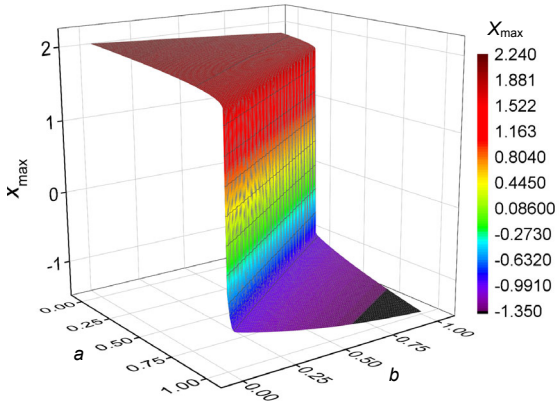

Fig. 11 Evolution of membrane potentials in the two-parameter space (membrane potentials for variable x in the neuron driven by photocurrent $i_S=I_0\arctan(x-u_a)$). The parameters are fixed at $I_0=0.05$, $u_a=0.1$, $c=0.1$, and $\xi=0.175$

When the phototube is handled as a current source, the neuron tends to present periodic firing modes and bifurcation analysis as shown in Fig. 12.

In fact, the neuron used to present periodic firing modes when the stimulus from the phototube connected to the neural circuit can be regarded as a continuous current source, and the firing modes become regular but with their parameters shifted greatly. In the same way, one parameter is shifted to detect the transition in the membrane potentials with the results shown in Fig. 13.

As presented in Fig. 13, appropriate switch and jump in any of the two intrinsic parameters (a, b) will induce transition from periodic to quiescent states. For example, periodic firing is generated at $a<0.8$, $b<0.4$ while the neuron becomes quiescent at $a>0.8$, $b>0.4$. That is, the physical property of the phototube and its outputs can control the excitability and firing modes of the functional neuron completely. Extensive numerical calculation is carried out, and it indicates that the Hamilton energy prefers higher values in the case of periodic firing modes.

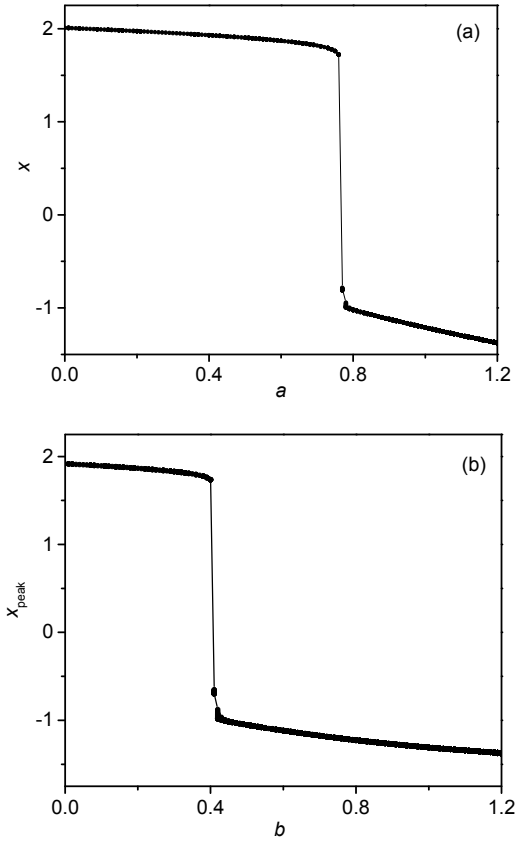

Fig. 12 Bifurcation diagrams for membrane potential x by changing one intrinsic parameter: (a) $b=0.32$; (b) $a=0.7$. The parameters are fixed at $I_0=0.05$, $u_a=0.1$, $c=0.1$, $\xi=0.175$, and the photocurrent is estimated at $i_S=I_0\arctan(x-u_a)$

In summary, most realistic optical signals often have wide bands, e.g. the chaotic signals are also generated with wide bands. The illumination and electromagnetic wave within certain frequency bands can be detected in the visual system by generating equivalent and effective electric stimuli in the neurons and neural circuit loop. Therefore, wave filtering becomes critical and the thresholds for frequency selection in the electromagnetic wave are relative to the physical property of the phototube (and of the retina in the visual system). In a practice, a variety of coating films can be coated and adhered to the photoelectric conversion device to select and/or filter illuminations within specific frequency bands. For the light-sensitive neural circuit/neuron, the equivalent

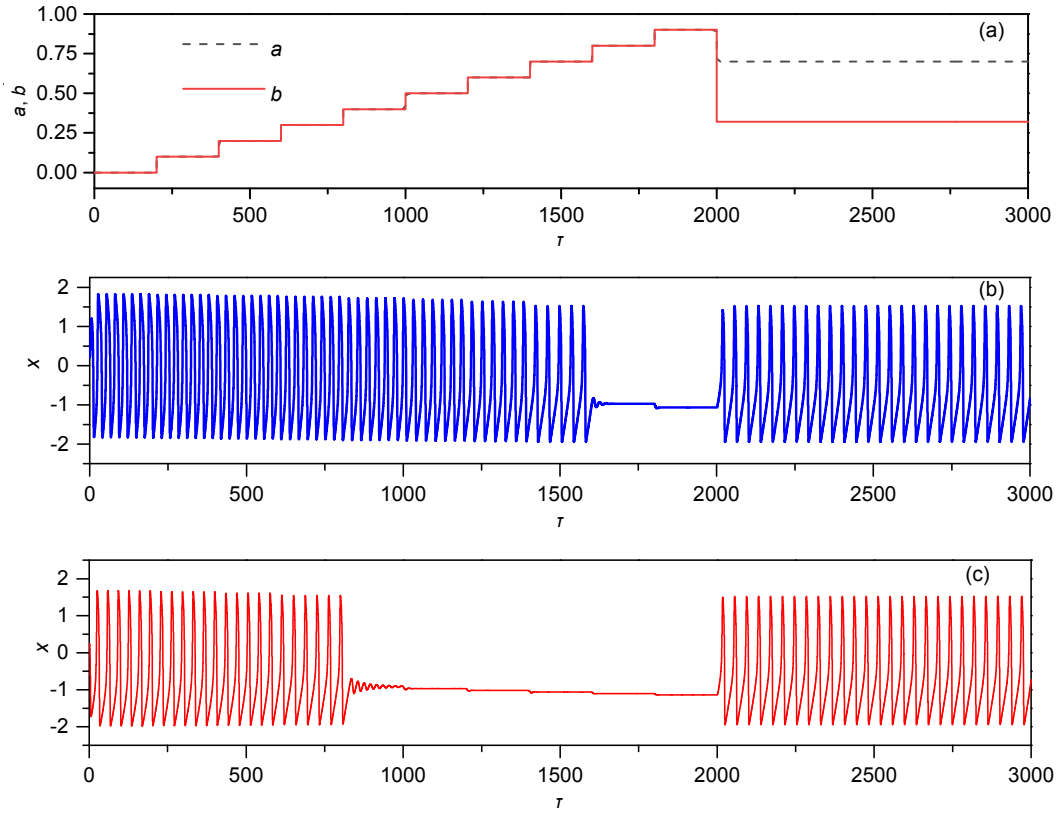

Fig. 13 Firing patterns in electric activities when two intrinsic parameters are jumped: (a) parameters jumping in constant steps with time; (b) jumped parameter a with fixed b=0.32; (c) jumped parameter b with fixed a=0.7. The other parameters are fixed at I_0=0.05, u_a=0.1, c=0.1, and ξ=0.175

photocurrent generated from the phototube can change the excitability and energy pumping effectively when the external illumination is filtered effectively. That is to say that the criterion for wave filtering and frequency selection well explains the potential biophysical mechanism for photoelectric conversion and coding in the visual system, and provides possible guidance for enhancing photoelectric conversion in artificial eyes and signal encoding in intelligent devices. Also, this proposal is effective in exploring wave filtering in auditory systems (Guo et al., 2021) because the ears can be sensitive to acoustic waves within specific frequency bands. In fact, electromagnetic radiation has an important impact on the wake-sleep cycle (Jin et al., 2019), and appropriate devices for filtering electromagnetic waves can be designed for ensuring healthy sleep. In experiments and extensive applications, the light-sensitive neural circuit can be excited by a silicon photocell, and a color absorber (filter) can be preplaced to select an optical wave with a suitable frequency band. Therefore, these light-sensitive neural circuits can be connected to build a network, which is capable of detecting optical signals and can control electric devices by using different illuminations. As reported in (Perc, 2007a, 2007b), the collective behaviors in the neural networks are controlled by the local excitability and connection topology, and adaptive adjusting in the coupling channels; links and local kinetics will be sensitive for detecting external stimuli and then appropriate wave propagation and energy flow can be controlled completely. Based on our proposal and criterion for wave filtering, more wave sources can be applied for detecting pattern formation, wave propagation, and energy flow in a network driven by filtered waves with spatiotemporal diversity.

4 Conclusions

Visual neurons are sensitive to electromagnetic waves and external illumination within specific

frequency bands, and the potential mechanism is that the retina can absorb certain bands of electromagnetic wave. In this paper, a phototube is incorporated into the neural circuit for improving its sensitivity to illumination and light. A criterion for wave filtering is suggested to select specific bands from a chaotic series, which is used to model a realistic signal source, and the filtered wave is effective in realizing photoelectric conversion via a phototube. As a result, the photocurrent across the phototube is dependent on the external illumination and filtered wave, and it is effective in triggering a variety of firing modes; the Hamilton energy is also adjusted effectively. This result can clarify the potential biophysical mechanism for signal processing and frequency selection in visual neurons, and the proposed criterion for wave filtering is also helpful for further designing artificial light-dependent and piezoelectric sensors and networks. For further investigation and application, appropriate coating films can be plated on the phototube and piezoelectric devices for wave filtering and selection of frequency, and then artificial functional sensors can be designed to perceive different physical signals.

Contributors

Xiu-fang ZHANG designed the research, processed the corresponding data, and wrote the first draft of the manuscript. Jun MA helped to organize the manuscript, and revised and edited the final version.

Conflict of interest

Xiu-fang ZHANG and Jun MA declare that they have no conflict of interest.

References

Achour SB, Pascual O, 2012. Astrocyte–neuron communication: functional consequences. *Neurochemical Research*, 37(11):2464-2473. https://doi.org/10.1007/s11064-012-0807-0

Babacan Y, Yesil A, Kacar F, 2017. Memristor emulator with tunable characteristic and its experimental results. *AEU-International Journal of Electronics and Communications*, 81:99-104. https://doi.org/10.1016/j.aeue.2017.07.012

Bao BC, Zhu YX, Ma J, et al., 2021. Memristive neuron model with an adapting synapse and its hardware experiments. *Science China Technological Sciences*, 64(5):1107-1117. https://doi.org/10.1007/s11431-020-1730-0

Bao H, Chen M, Wu HG, et al., 2020. Memristor initial-boosted coexisting plane bifurcations and its extreme multi-stability reconstitution in two-memristor-based dynamical system. *Science China Technological Sciences*, 63(4):603-613. https://doi.org/10.1007/s11431-019-1450-6

Baysal V, Erkan E, Yilmaz E, 2021. Impacts of autapse on chaotic resonance in single neurons and small-world neuronal networks. *Philosophical Transactions of the Royal Society A: Mathematical, Physical and Engineering Sciences*, 379(2198):20200237. https://doi.org/10.1098/rsta.2020.0237

Brazhe AR, Postnov DE, Sosnovtseva O, 2018. Astrocyte calcium signaling: interplay between structural and dynamical patterns. *Chaos*, 28(10):106320. https://doi.org/10.1063/1.5037153

Chen M, Qi JW, Wu HG, et al., 2020. Bifurcation analyses and hardware experiments for bursting dynamics in non-autonomous memristive FitzHugh-Nagumo circuit. *Science China Technological Sciences*, 63(6):1035-1044. https://doi.org/10.1007/s11431-019-1458-5

Dipoppa M, Ranson A, Krumin M, et al., 2018. Vision and locomotion shape the interactions between neuron types in mouse visual cortex. *Neuron*, 98(3):602-615. https://doi.org/10.1016/j.neuron.2018.03.037

Du MM, Li JJ, Yuan ZX, et al., 2020. Astrocyte and ions metabolism during epileptogenesis: a review for modeling studies. *Chinese Physics B*, 29(3):038701. https://doi.org/10.1088/1674-1056/ab6961

Duan KR, Fong S, Chen CLP, 2020. Multilayer neural networks-based control of underwater vehicles with uncertain dynamics and disturbances. *Nonlinear Dynamics*, 100(4):3555-3573. https://doi.org/10.1007/s11071-020-05720-5

Erkan Y, Saraç Z, Yılmaz E, 2019. Effects of astrocyte on weak signal detection performance of Hodgkin–Huxley neuron. *Nonlinear Dynamics*, 95(4):3411-3421. https://doi.org/10.1007/s11071-019-04764-6

Fitch AL, Yu DS, Iu HHC, et al., 2012. Hyperchaos in a memristor-based modified canonical Chua's circuit. *International Journal of Bifurcation and Chaos*, 22(6):1250133. https://doi.org/10.1142/S0218127412501337

Furtak SC, Ahmed OJ, Burwell RD, 2012. Single neuron activity and theta modulation in postrhinal cortex during visual object discrimination. *Neuron*, 76(5):976-988. https://doi.org/10.1016/j.neuron.2012.10.039

Gabbiani F, Krapp HG, Koch C, et al., 2002. Multiplicative computation in a visual neuron sensitive to looming. *Nature*, 420(6913):320-324. https://doi.org/10.1038/nature01190

Ge MY, Jia Y, Xu Y, et al., 2019. Wave propagation and synchronization induced by chemical autapse in chain Hindmarsh–Rose neural network. *Applied Mathematics and Computation*, 352:136-145. https://doi.org/10.1016/j.amc.2019.01.059

Guo SL, Tang J, Ma J, et al., 2017. Autaptic modulation

of electrical activity in a network of neuron-coupled astrocyte. *Complexity*, 2017:4631602. https://doi.org/10.1155/2017/4631602

Guo YT, Zhou P, Yao Z, et al., 2021. Biophysical mechanism of signal encoding in an auditory neuron. *Nonlinear Dynamics*, 1-12. https://doi.org/10.1007/s11071-021-06770-z

Heil P, 2004. First-spike latency of auditory neurons revisited. *Current Opinion in Neurobiology*, 14(4):461-467. https://doi.org/10.1016/j.conb.2004.07.002

Ibrahim O, Hassan SM, Abdulkarim A, et al., 2019. Design of wheatstone bridge based thermistor signal conditioning circuit for temperature measurement. *Journal of Engineering Science and Technology Review*, 12(1):12-17. https://doi.org/10.25103/jestr.121.02

Jiao TC, Zong GD, Ahn CK, 2020. Noise-to-state practical stability and stabilization of random neural networks. *Nonlinear Dynamics*, 100(3):2469-2481. https://doi.org/10.1007/s11071-020-05628-0

Jin WY, Wang A, Ma J, et al., 2019. Effects of electromagnetic induction and noise on the regulation of sleep wake cycle. *Science China Technological Sciences*, 62(12): 2113-2119. https://doi.org/10.1007/s11431-018-9423-x

Juzekaeva E, Nasretdinov A, Battistoni S, et al., 2019. Coupling cortical neurons through electronic memristive synapse. *Advanced Materials Technologies*, 4(1):1800350. https://doi.org/10.1002/admt.201800350

Koudafokê GN, Hinvi LA, Miwadinou CH, et al., 2021. Passive sensor with Josephson junction coupled to an electric resonator and a nanobeam. *Sensors and Actuators A: Physical*, 318:112509. https://doi.org/10.1016/j.sna.2020.112509

Koundakjian EJ, Appler JL, Goodrich LV, 2007. Auditory neurons make stereotyped wiring decisions before maturation of their targets. *Journal of Neuroscience*, 27(51): 14078-14088. https://doi.org/10.1523/JNEUROSCI.3765-07.2007

Kyprianidis IM, Papachristou V, Stouboulos IN, et al., 2012. Dynamics of coupled chaotic Bonhoeffer–van der Pol oscillators. *WSEAS Transactions on Systems*, 11(9):516-526.

Lee SJ, Kenyon C, 2009. Regulation of the longevity response to temperature by thermosensory neurons in *Caenorhabditis elegans*. *Current Biology*, 19(9):715-722. https://doi.org/10.1016/j.cub.2009.03.041

Li JJ, Wang R, Du MM, et al., 2016. Dynamic transition on the seizure-like neuronal activity by astrocytic calcium channel block. *Chaos, Solitons & Fractals*, 91:702-708. https://doi.org/10.1016/j.chaos.2016.08.009

Li YY, Gu HG, Jia B, et al., 2021. The nonlinear mechanism for the same responses of neuronal bursting to opposite self-feedback modulations of autapse. *Science China Technological Sciences*, 64(7):1459-1471. https://doi.org/10.1007/s11431-020-1753-y

Liu Y, Xu WJ, Ma J, et al., 2020a. A new photosensitive neuron model and its dynamics. *Frontiers of Information Technology & Electronic Engineering*, 21(9):1387-1396. https://doi.org/10.1631/FITEE.1900606

Liu Y, Xu Y, Ma J, 2020b. Synchronization and spatial patterns in a light-dependent neural network. *Communications in Nonlinear Science and Numerical Simulation*, 89:105297. https://doi.org/10.1016/j.cnsns.2020.105297

Lukić J, Denić D, 2015. A novel design of an NTC thermistor linearization circuit. *Metrology and Measurement Systems*, 22(3):351-362. https://doi.org/10.1515/mms-2015-0035

Lv M, Ma J, Yao YG, et al., 2019. Synchronization and wave propagation in neuronal network under field coupling. *Science China Technological Sciences*, 62(3):448-457. https://doi.org/10.1007/s11431-018-9268-2

Ma J, Qin HX, Song XL, et al., 2015. Pattern selection in neuronal network driven by electric autapses with diversity in time delays. *International Journal of Modern Physics B*, 29(1):1450239. https://doi.org/10.1142/S0217979214502397

Ma J, Yang ZQ, Yang LJ, et al., 2019. A physical view of computational neurodynamics. *Journal of Zhejiang University-SCIENCE A (Applied Physics & Engineering)*, 20(9):639-659. https://doi.org/10.1631/jzus.A1900273

Machens CK, Schütze H, Franz A, et al., 2003. Single auditory neurons rapidly discriminate conspecific communication signals. *Nature Neuroscience*, 6(4):341-342. https://doi.org/10.1038/nn1036

MacVicar BA, Newman EA, 2015. Astrocyte regulation of blood flow in the brain. *Cold Spring Harbor Perspectives in Biology*, 7(5):a020388. https://doi.org/10.1101/cshperspect.a020388

Nakayama T, 1985. Thermosensitive neurons in the brain. *The Japanese Journal of Physiology*, 35(3):375-389. https://doi.org/10.2170/jjphysiol.35.375

Perc M, 2007a. Effects of small-world connectivity on noise-induced temporal and spatial order in neural media. *Chaos, Solitons & Fractals*, 31(2):280-291. https://doi.org/10.1016/j.chaos.2005.10.018

Perc M, 2007b. Fluctuating excitability: a mechanism for self-sustained information flow in excitable arrays. *Chaos, Solitons & Fractals*, 32(3):1118-1124. https://doi.org/10.1016/j.chaos.2005.11.035

Peron S, Gabbiani F, 2009. Spike frequency adaptation mediates looming stimulus selectivity in a collision-detecting neuron. *Nature Neuroscience*, 12(3):318-326. https://doi.org/10.1038/nn.2259

Pikovskii AS, Rabinovich MI, 1978. A simple autogenerator with stochastic behavior. *Soviet Physics Doklady*, 23: 183-185.

Pountougnigni OV, Yamapi R, Filatrella G, et al., 2019. Noise and disorder effects in a series of birhythmic Josephson junctions coupled to a resonator. *Physical Review E*, 99(3):032220.

https://doi.org/10.1103/PhysRevE.99.032220

Qin HX, Ma J, Wang CN, et al., 2014. Autapse-induced target wave, spiral wave in regular network of neurons. *Science China Physics, Mechanics & Astronomy*, 57(10):1918-1926. https://doi.org/10.1007/s11433-014-5466-5

Richter CP, Bayon R, Izzo AD, et al., 2008. Optical stimulation of auditory neurons: effects of acute and chronic deafening. *Hearing Research*, 242(1-2):42-51. https://doi.org/10.1016/j.heares.2008.01.011

Ruchty M, Roces F, Kleineidam CJ, 2010. Detection of minute temperature transients by thermosensitive neurons in ants. *Journal of Neurophysiology*, 104(3):1249-1256. https://doi.org/10.1152/jn.00390.2010

Saira OP, Zgirski M, Viisanen KL, et al., 2016. Dispersive thermometry with a Josephson junction coupled to a resonator. *Physical Review Applied*, 6(2):024005. https://doi.org/10.1103/PhysRevApplied.6.024005

Seung HS, Lee DD, Reis BY, et al., 2000. The autapse: a simple illustration of short-term analog memory storage by tuned synaptic feedback. *Journal of Computational Neuroscience*, 9(2):171-185. https://doi.org/10.1023/A:1008971908649

Song XL, Wang HT, Chen Y, 2019. Autapse-induced firing patterns transitions in the Morris–Lecar neuron model. *Nonlinear Dynamics*, 96(4):2341-2350. https://doi.org/10.1007/s11071-019-04925-7

Tang J, Zhang J, Ma J, et al., 2017. Astrocyte calcium wave induces seizure-like behavior in neuron network. *Science China Technological Sciences*, 60(7):1011-1018. https://doi.org/10.1007/s11431-016-0293-9

Vourkas I, Sirakoulis GC, 2016. Emerging memristor-based logic circuit design approaches: a review. *IEEE Circuits and Systems Magazine*, 16(3):15-30. https://doi.org/10.1109/MCAS.2016.2583673

Wang CN, Guo SL, Xu Y, et al., 2017. Formation of autapse connected to neuron and its biological function. *Complexity*, 2017:5436737. https://doi.org/10.1155/2017/5436737

Wang CN, Tang J, Ma J, 2019. Minireview on signal exchange between nonlinear circuits and neurons via field coupling. *The European Physical Journal Special Topics*, 228(10):1907-1924. https://doi.org/10.1140/epjst/e2019-800193-8

Wiederman SD, O'Carroll DC, 2013. Selective attention in an insect visual neuron. *Current Biology*, 23(2):156-161. https://doi.org/10.1016/j.cub.2012.11.048

Wu FQ, Zhang Y, Zhang XJ, 2019. Regulating firing rates in a neural circuit by activating memristive synapse with magnetic coupling. *Nonlinear Dynamics*, 98(2):971-984. https://doi.org/10.1007/s11071-019-05239-4

Wu FQ, Ma J, Zhang G, 2020. Energy estimation and coupling synchronization between biophysical neurons. *Science China Technological Sciences*, 63(4):625-636. https://doi.org/10.1007/s11431-019-9670-1

Xu Y, Liu MH, Zhu ZG, et al., 2020a. Dynamics and coherence resonance in a thermosensitive neuron driven by photocurrent. *Chinese Physics B*, 29(9):098704. https://doi.org/10.1088/1674-1056/ab9dee

Xu Y, Guo YY, Ren GD, et al., 2020b. Dynamics and stochastic resonance in a thermosensitive neuron. *Applied Mathematics and Computation*, 385:125427. https://doi.org/10.1016/j.amc.2020.125427

Yao CG, 2020. Synchronization and multistability in the coupled neurons with propagation and processing delays. *Nonlinear Dynamics*, 101(4):2401-2411. https://doi.org/10.1007/s11071-020-05922-x

Yao CG, He ZW, Nakano T, et al., 2019. Inhibitory-autapse-enhanced signal transmission in neural networks. *Nonlinear Dynamics*, 97(2):1425-1437. https://doi.org/10.1007/s11071-019-05060-z

Zandi-Mehran N, Jafari S, Golpayegani SMRH, et al., 2020. Different synaptic connections evoke different firing patterns in neurons subject to an electromagnetic field. *Nonlinear Dynamics*, 100(2):1809-1824. https://doi.org/10.1007/s11071-020-05576-9

Zhang L, Jones S, Brody K, et al., 2004. Thermosensitive transient receptor potential channels in vagal afferent neurons of the mouse. *American Journal of Physiology-Gastrointestinal and Liver Physiology*, 286(6):G983-G991. https://doi.org/10.1152/ajpgi.00441.2003

Zhang Y, Xu Y, Yao Z, et al., 2020. A feasible neuron for estimating the magnetic field effect. *Nonlinear Dynamics*, 102(3):1849-1867. https://doi.org/10.1007/s11071-020-05991-y

Zhang Y, Zhou P, Tang J, et al., 2021. Mode selection in a neuron driven by Josephson junction current in presence of magnetic field. *Chinese Journal of Physics*, 71:72-84. https://doi.org/10.1016/j.cjph.2020.11.011

Zhao ZG, Li L, Gu HG, 2020. Excitatory autapse induces different cases of reduced neuronal firing activities near Hopf bifurcation. *Communications in Nonlinear Science and Numerical Simulation*, 85:105250. https://doi.org/10.1016/j.cnsns.2020.105250

Zhou P, Yao Z, Ma J, et al., 2021a. A piezoelectric sensing neuron and resonance synchronization between auditory neurons under stimulus. *Chaos, Solitons & Fractals*, 145:110751. https://doi.org/10.1016/j.chaos.2021.110751

Zhou P, Hu XK, Zhu ZG, et al., 2021b. What is the most suitable Lyapunov function? *Chaos, Solitons & Fractals*, 150:111154. https://doi.org/10.1016/j.chaos.2021.111154